Palaeomagnetic evidence and tectonic origin of clockwise rotations in the Yangtze fold belt, South China Block

Tan Xiaodong, Kodama Kennethp., Stuart A. Gilder, Vincent Courtillot, Jean-Pascal Cogné

Geophys. J. Int. (2007) **168,** 48–58 doi: 10.1111/j.1365-246X.2006.03195.x

Palaeomagnetic evidence and tectonic origin of clockwise rotations in the Yangtze fold belt, South China Block

Xiaodong Tan,[1] Kenneth P. Kodama,[2] Stuart Gilder,[3,*] Vincent Courtillot[3] and Jean-Pascal Cogné[3]

[1]*CAS Key Laboratory of Marginal Sea Geology, South China Sea Institute of Oceanology, Chinese Academy of Sciences,* 164 *West Xin Gang Road, Guangzhou* 510301, *China. E-mail: xdtan@scsio.ac.cn*
[2]*Department of Earth and Environmental Sciences, Lehigh University,* 31 *Williams Dr, Bethlehem,* PA 18015, *USA*
[3]*Institut de Physique du Globe de Paris, Laboratoir de Paléomagnétisme,* 4 *place Jussieu,* 75252 *Paris cedex* 05*, France*

Accepted 2006 August 9. Received 2006 August 9; in original form 2006 May 30

SUMMARY

Fold axis strikes in the Yangtze fold belt of the South China Block (SCB) undergo significant changes over distances of >1000 km. This large-scale variation provides an ideal opportunity to test the oroclinal-bending hypothesis using palaeomagnetic methods, which we have attempted by drilling the Lower Triassic Daye Formation limestones in western Hubei Province. Thermal demagnetization isolated two components in most samples. A low unblocking temperature component (<350 °C) that does not decay to the origin is interpreted as a drilling induced magnetization. The second, high temperature component (HTC), isolated at temperatures >400 °C, unblocks univectorially towards the origin. The HTC passes the McFadden-fold test with an overall mean tilt-corrected direction of Dec = 255°, Inc = −24° ($N = 7, \alpha_{95} = 9°$). Scanning electron microscopy (SEM) observations suggest an early diagenetic, possible (bio)chemical origin for the magnetic extracts dominated by Ti-poor magnetite. Rock magnetic data show no evidence that the HTC has been affected by tectonic or compaction strain. Our data together with previously published results suggest a general clockwise rotation pattern in the Middle Yangtze fold belt, which is probably related to the collision between the North and SCBs. Comparison of palaeomagnetic rotations with fold axis trends in the fold belt suggests that about 30° clockwise rotation occurred in the Middle reaches of the Yangtze River, while a 15° difference in fold axis trends would be due to initial variation within the fold belt. However, since little is known about the timing of the clockwise rotation, whether the Middle Yangtze fold belt is an orocline awaits further studies.

Key words: Mesozoic, oroclinal bending, palaeomagnetic rotation, South China Block, Yangtze fold belt.

INTRODUCTION

China is composed of several plates, of which the North China Block (NCB) and South China Block (SCB) comprise the two largest. In one of the original palaeomagnetic studies applied to the tectonics of China, McElhinny *et al.* (1981) found that the Late Permian poles for the NCB and SCB were quite discordant, suggesting that the two blocks had been far from their present relative positions at that time. Since then, further palaeomagnetic studies have refined our understanding of their kinematic history. Lin *et al.* (1985) constructed the first apparent polar wander path (APWP) for these two blocks, and concluded that suturing of the NCB and SCB occurred during the interval between the Middle Triassic and the Middle Jurassic. Current models of collision and suturing largely follow the work of Zhao & Coe (1987) who suggested that the NCB and SCB first collided in the Late Permian near the eastern part of the two blocks, and continued colliding in a scissor-like fashion as the NCB rotated counter-clockwise with respect to the SCB about a pivot point centred around the initial point of collision. More recent palaeomagnetic studies have improved the APWPs and refined the kinematic models related to suturing (e.g. Fang *et al.* 1990; Yang *et al.* 1991, 1992; Gilder & Courtillot 1997; Gilder *et al.* 1999; Yang & Besse 2001).

Several prominent, often large-scale features resulting from the NCB–SCB collision are well preserved (Fig. 1). One is the presence

*Now at: Ludwig Maximilians University, Department of Earth and Environmental Sciences, Geophysics Section, Theresienstr. 41, 80333 Munich, Germany.

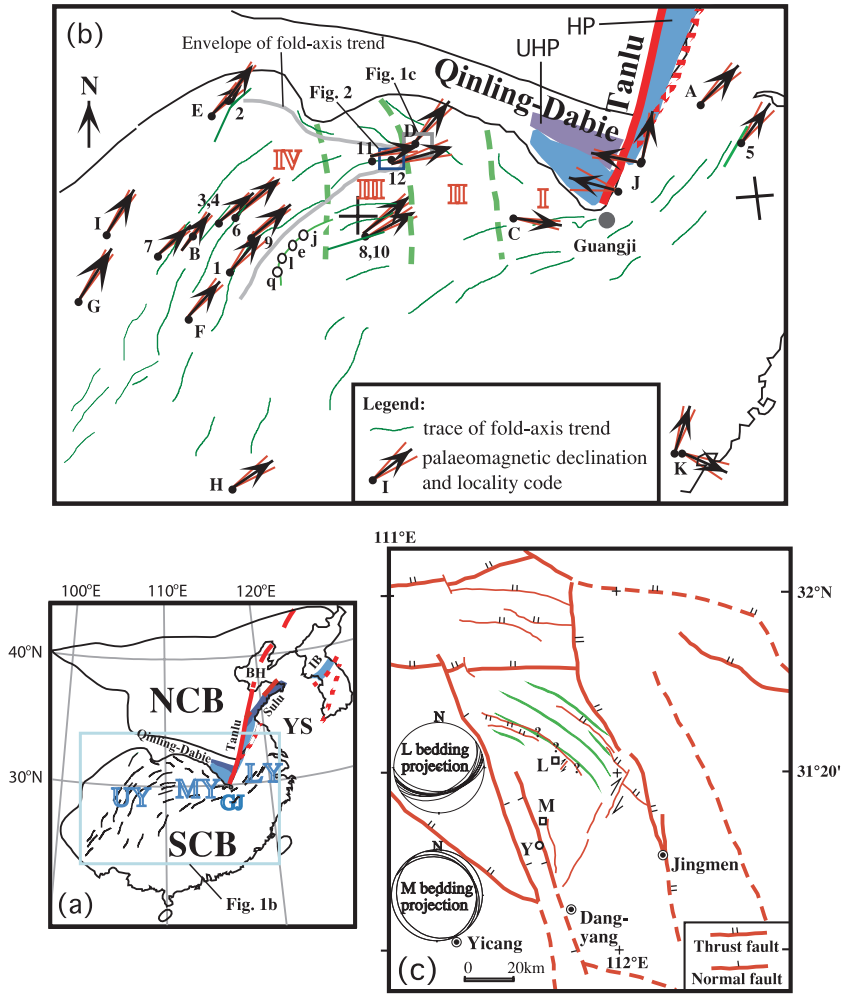

Figure 1. (a) Present configuration of North China Block (NCB) and South China Block (SCB) showing the Qinling–Dabie, Tanlu, Sulu and Imjingang (IB) suture zones and variations of fold-axis strikes (thin solid lines) in the Yangtze fold belt and (b) latest Permian to Middle Triassic palaeomagnetic declinations from various localities (Table 2). BH, Bohai Bay; YS, Yellow Sea; GJ, Guangji; HP and UHP, high-pressure and ultrahigh-pressure metamorphic suits in Dabie Shan and Sulu suture zone; UY, MY and LY, Upper, Middle and Lower Yangtze regions. Jurassic stratigraphic subdivisions (BGMRHP 1990): I, Puqi-Daye; II, Jingmen–Dangyang; III, Lichuan-Zigui and IV, Northern Sichuan. (c) Major faults surrounding the Jingmen–Dangyang basin (locality D in (b) studied by Huang & Opdyke 1997). Also shown are equal area projections of the bedding planes at the two sections M, Maoping; L, Liujiatai and Y, Yuan'an cities.

of coesite- and diamond-bearing ultrahigh pressure metamorphic (UHPM) units in the Dabie Shan and Sulu regions (Fig. 1a). The UHPM units are separated by more than 500 km across the Tanlu fault, which is abruptly terminated south of the Dabie Shan and north of the mid-Yangtze fold belt (Xu 1993). Another prominent feature is the presence of >1000-km-long folds that follow the western and northern limit of the Yangtze fold belt (Fig. 1b) (Academia Sinica 1976). On the first-order, fold axes trend approximately NE–SW in the west (the Upper Yangtze fold belt), E–W in the north (Middle Yangtze) and NNE–SSW in the east (Lower Yangtze) regions (Fig. 1). Gilder *et al.* (1999) explained the origin of this pattern of changing fold axis trends by a two-phase process. The first phase would have been due to the NCB–SCB collision, with Dabieshan acting as a rigid indenter that penetrated the SCB. Folds were produced along the indenter contours in the middle and lower parts of the Yangtze fold belt (Fig. 1b). The second phase would have occurred due to the India–Asia collision, which pushed Tibet eastwards against the SCB. Thrusting during Tibet–SCB shortening would have created the Longmenshan range and the NE-trending folds in the Upper Yangtze fold belt.

Huang & Opdyke (1996) reported palaeomagnetic results of Middle Triassic red beds from three localities (8, 10 and 11, in Fig. 1b) in the Middle Yangtze fold belt where palaeomagnetic declinations point more easterly than those from other areas, roughly parallel to the E–W trending fold axes. Further palaeomagnetic study north of these three localities (locality D, Fig. 1b), closer to the Qinling suture, showed northerly palaeomagnetic declinations that were highly oblique to the fold axes, thus refuting an oroclinal-bending model for the Middle Yangtze fold belt and suggesting that the rotations were not related to the NCB–SCB collision (Huang & Opdyke 1997). Yang & Besse (2001) tested the oroclinal-rotation hypothesis in the Yangtze fold belt by comparing palaeomagnetic declinations and strike directions for three geological periods: latest Permian to earliest Triassic, Early Triassic and Middle Triassic. They found no direct correlation between the two for any age and concluded that the curvature of the fold axis in the Yangtze fold belt was not due to oroclinal bending. To further test the pattern of palaeomagnetic rotations in the Yangtze fold belt, we performed a palaeomagnetic study of Lower Triassic limestones from the Zigui syncline, west Hubei province (locality 12 in Fig. 1b) and re-analysed the existing

palaeomagnetic and structural data. We find that the majority of palaeomagnetic data from Middle Yangtze fold belt can be fitted into a general clockwise rotation pattern. This pattern is compatible with a model of NCB indentation that facilitates both finite block rotation and long wavelength folding that is partially obscured by initial variability (pre-rotation) of fold axis trends.

GEOLOGY AND SAMPLING

While most workers agree that the NCB–SCB collision occurred from the Permian through at least the Middle Jurassic (e.g. Zhao & Coe 1987; Gilder *et al.* 1999), the stratigraphy throughout the Yangtze fold belt only records deformation occurring at the latest stages of suturing. In Hubei Province (I and II in Fig. 1b), Triassic to Middle Jurassic deposits appears to be conformable. A folding event occurred in region I (Fig. 1b) is marked by an unconformity between the Majiashan and Huajiahu formations. Volcanic rocks in the upper part of the Majiashan Formation were radiometrically dated as 144 Ma, and the underlying Huajiahu Fm was intruded by granite dated at 160 Ma thus constraining the age of the angular unconformity to be between 144 and 160 Ma (BGMRHP 1990, p. 207 and 557). This age of deformation is similar to the Late/Middle Jurassic unconformity described in Gilder & Courtillot (1997). However, younger unconformities in the same region have been identified between the Upper Jurassic and Early Cretaceous (BGMRHP 1990, p. 225; Geologic map) although their associations with the NCB–SCB collision are unclear. In southeastern Sichuan and westernmost Hubei provinces (localities q, l, e and j, Fig. 1b), the flat-lying Upper Cretaceous Zhengyang Fm. rests on steeply dipping Middle Jurassic and older sedimentary sequences (BGMRHP 1990; BGMRSP 1991). Therefore, folding in these areas occurred between the Middle Jurassic and Upper Cretaceous.

Our study area is situated at the eastern end of the major regional EW trending fold in the Middle Yangtze fold belt (locality 12, Fig. 1b) and, at a more local scale, at the eastern end of the NS trending Zigui syncline (section XT and XJ, Fig. 2) (BGMRHP 1990). Based on Huang and Opdyke's (1996) structural data from Badong County (locality 11), the large EW trending fold plunges 25° towards the east. At a larger scale, the Zigui syncline is located on the western edge of the dome-like Huangling anticline. Palaeomagnetic declinations of the Zigui syncline isolated from the Middle Triassic Badong Formation (Badong County, locality 11) point easterly, compatible with an oroclinal-bending model, while declinations from the Jingmen–Dangyang basin (site D, 110 km east of the study area) are NE oriented, consistent with the declinations from other parts of the Yangtze block (Huang & Opdyke 1996, 1997). Because the latter site lies closer to the Qinling suture and is not rotated, Huang & Opdyke (1997) suggested that the mechanism responsible for all the rotations in the Middle Yangtze fold belt were not related to the NCB–SCB collision. Our sampling locality lies between localities D and 11, 40 km east of locality 11 (Fig. 1b). Locally, the sampling sites are located on a monocline, which dips 25°–35° to the WNW (Fig. 2). There are at least two stages of deformation. One is NS directed convergence, shown by EW trending

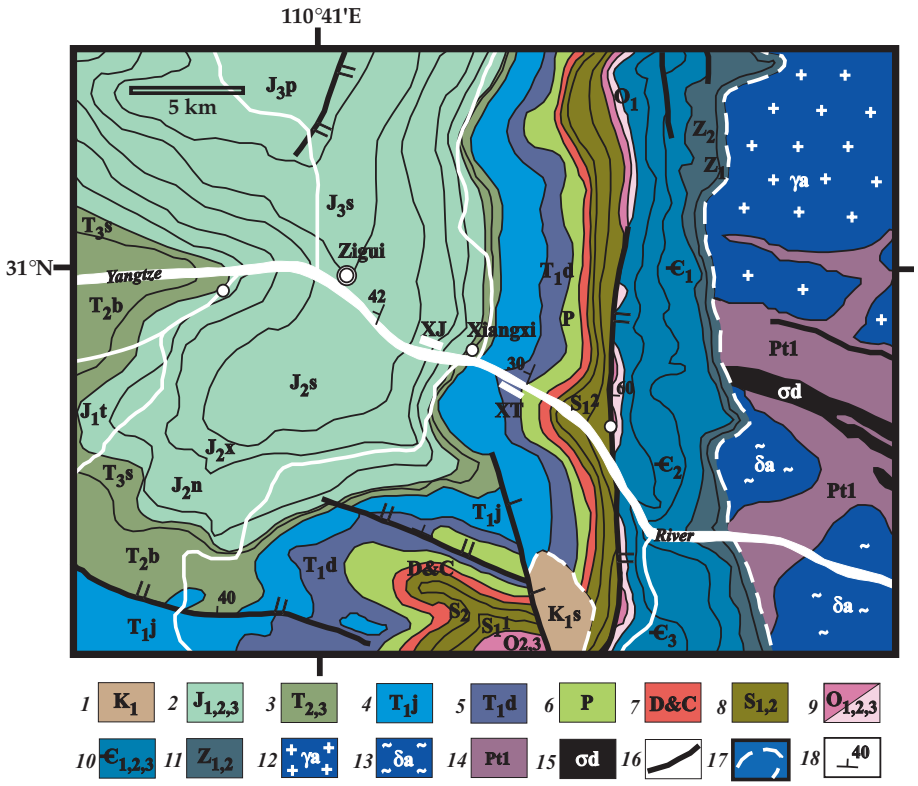

Figure 2. A geological map of the study area (redrawn from BGMRHP 1990). 12–15 are crystalline basement rocks. The Upper Proterozoic (Sinian, 11) is the first cover sequence of the Yangtze platform, including terrigenous and glacial deposits in the lower part, and marine deposits (carbonate and shale) in the upper part. Palaeozoic and Lower Triassic are mainly composed of marine deposits: 10, Cambrian; 9, Ordovician; 8, Silurian; 7, Devonian and Carboniferous; 6, Permian and 5, Triassic Daye and 4, Jianglingjiang formations. The younger sediments are composed of continental alluvial, fluvial and lacustrine deposits: 3, Middle and Upper Triassic, 2, Jurassic and 1, Lower Cretaceous. 16, faults, sense of faulting is the same as in Fig. 1(c); 17, unconformity and 18, attitude with dip angle of fault or bedding plane. XT and XJ are the Triassic and Jurassic sampled sections, respectively.

thrust faults, followed by a nearly EW directed convergence. The first deformation phase caused the major EW trending folds and the latter apparently formed the Zigui syncline. Because locality 11 yielded the largest palaeomagnetic rotation, which places the greatest weight in correlation analysis between palaeomagnetic rotation and fold axis trend, our study area is critical to test (1) whether the declination of locality 11 could reflect a local vertical axis rotation and (2) the palaeomagnetic rotation pattern in the Middle Yangtze region.

Using a portable gasoline-powered drill, we collected 75 samples from 10 sites of the Lower Triassic Daye Formation along the southern bank of the Yangtze Gorge, in Xiangxi County, Hubei Province (XT on Fig. 2). Samples were oriented with a magnetic compass. Cores were drilled in a 100-m-thick series of thin to medium-thick bedded limestones at the lower part of the formation. Just below is a 5-m-thick layer of marl, shale and mudstones, which yields a typical Early Triassic *Claraia wangi (pelecypoda)* assemblage, corresponding to the Induan stage (Yang *et al.* 1986; BGMRHP 1990). We also sampled 10 sites (80 samples) of Middle Jurassic Niejiashan and Xiashaximiao Formation, grey to yellow sandstone, 3 km west of the Triassic section (XJ on Fig. 2).

PALAEOMAGNETISM

62 samples from seven Early Triassic sites and 43 samples from six Middle Jurassic sites were measured at Lehigh University, of which two samples per site were subjected to detailed thermal and alternating field demagnetization. The Jurassic samples only display present-day field directions (Dec $= -3°$, Inc $= 46°$) in *in situ* coordinates, and the remanence at high temperatures ($>300\,°C$) is noisy and unstable. Recent geomagnetic field remagnetizations of Jurassic clastic deposits are commonly observed in the Yangtze block (e.g. chapter 3 in Enkin 1990). Thermal demagnetization successfully isolated dual component magnetizations in the Triassic limestones, while alternating field demagnetization failed to do so, and thus, the remaining samples were thermally demagnetized using seven to nine steps up to 575 °C. The remanent magnetization components of each sample were calculated by principal component analysis (Kirschvink 1980). The mean direction of each site and the mean of the site means were calculated by Fisher statistics (Fisher 1953).

The *in situ* natural remanent magnetizations (NRM) have shallow inclinations with westerly declinations (Figs 3 and 4a). A low temperature component (LTC) is resolved at unblocking temperatures $<250\,°C$, while a high temperature component (HTC) is isolated at unblocking temperatures $>400\,°C$ (Fig. 3), with overlapping spectra of the two components occurring between 250 and 400 °C. The *in situ* LTC directions are highly scattered around the vertical axis with steep positive inclinations (Fig. 4b and Table 1). The *in situ* LTC inclinations are correlated with the plunges of sample cores (Fig. 4f). Therefore, the LTC was probably created during sampling, similar to that observed by Tan *et al.* (2000). The HTC points WSW with a shallow and negative inclination (Figs 4c–e). The overall *in situ* site mean HTC direction is Dec $= 262°$, Inc $= -8°$ ($\alpha_{95} = 10°$, $N = 7$), and that for tilt-corrected coordinates is Dec $= 255°$, Inc $= -24°$ ($\alpha_{95} = 9°$) (Table 1). The precision parameter (k) for the overall site mean direction, increases monotonically from 35 at 0 per cent to 44 at 100 per cent unfolding. Because bedding attitudes do not vary significantly, we applied the McFadden (1990) fold test, which yielded a ξ_2 statistical parameter of 3.673 in geographic coordinates, which is greater than the critical value (ξ_c) of 3.086 at the

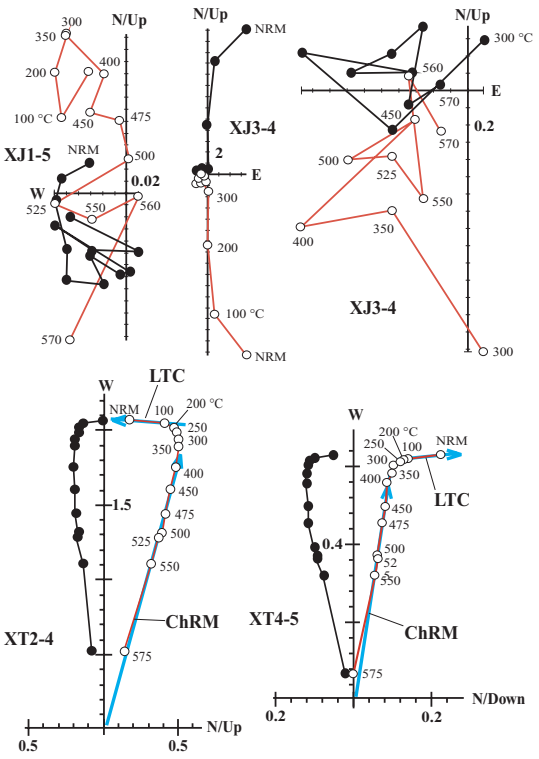

Figure 3. Zijderveld (1967) diagrams showing thermal demagnetization path. Solid circles denote the projection of magnetization vectors onto the north and east coordinates, and open circles denote the projection in vertical coordinates. Units in mA m^{-1}.

95 per cent confidence level. This suggests that the *in situ* mean direction is correlated with geographic coordinates and the HTC was not acquired after tilting. In stratigraphic coordinates, ξ_2(=2.348) is less than ξ_c, so the tilt-corrected mean HTC direction is not correlated with bedding attitudes (Fig. 5). Thus the McFadden-fold test suggests that the HTC was acquired before folding.

We also applied the Watson & Enkin (1993) OC fold test and Enkin (2003) DC fold test. Assuming a 3° uncertainty of bedding orientations, in 1000 simulations of OC test, the best precision parameter of the overall mean HTC direction occurred at 118 ± 50 per cent tilt correction. However, the test is sensitive to the uncertainty of bedding orientations. The DC fold test is indeterminate, because the site-mean HTC directions are too scattered and/or the bedding structures are too small. Enkin (2003) pointed out that for the DC test to be the most effective, the α_{95} of overall mean direction should be less than 1/6 of bedding attitude difference. Indeed, the α_{95} of the overall mean HTC direction (9°, in the stratigraphic coordinates) is much greater than 1/6 of the largest difference (22°) in bedding attitudes. Therefore, failure of the DC test is due to small variation in our bedding structures.

Furthermore, we performed consistency tests for our HTC data. Huang & Opdyke (1996) reported palaeomagnetic data of the Middle Triassic Badong Formation from the western flank of the Zigui syncline. According to Yang & Besse (2001), the Early Triassic and Middle Triassic reference poles for SCB are 43.8°N, 213.8°E ($A_{95} = 3.5°$) and 42.7°N, 212.6°E ($A_{95} = 6.0°$), respectively. These poles are indistinguishable at 95 per cent confidence level, rendering reasonable consistency tests for the Early and Middle Triassic palaeomagnetic results from the Zigui syncline. Together, the 23 sites (seven Early Triassic and 16 Middle Triassic) yielded mean

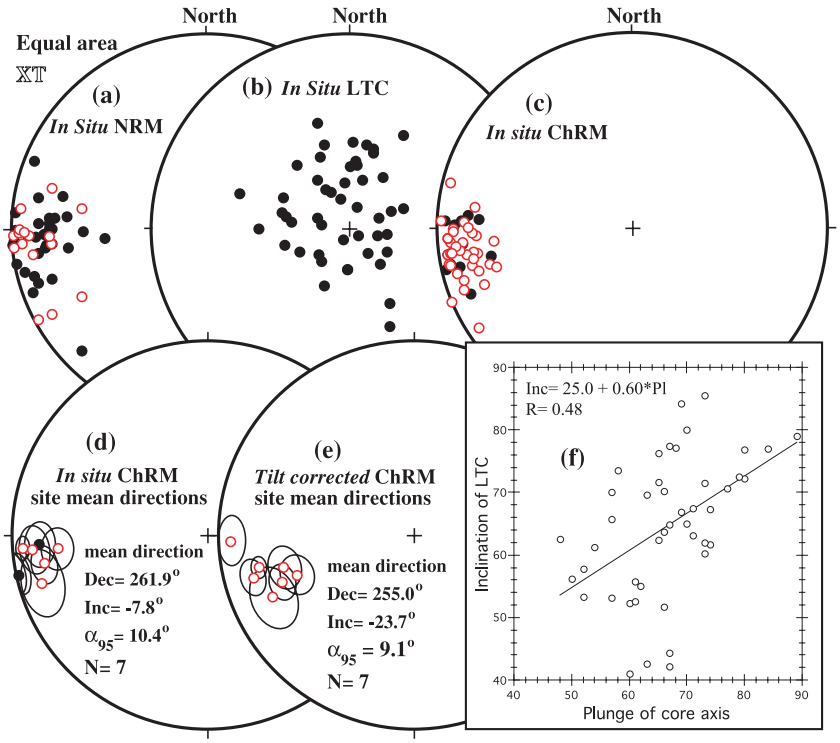

Figure 4. Equal area stereonet projection of remanent magnetization components, showing (a) *in situ* westerly and shallow NRM directions, (b) scattered steep LT component, (c) and (d) westerly more negative *in situ* ChRMs and (e) tilt corrected site mean ChRMs. Also shown is the correlation between LTC inclination and sample plunge (f).

Table 1. Statistical results of remanent magnetization components of Early Triassic limestones, Daye Formation, Xiangxi County, Hubei Province, China.

Site	Comp	Dg (°)	Ig (°)	Strike (°)	Dip (°)	Ds (°)	Is (°)	n/N	κ	α_{95}(°)
XT6	LTC	133.3	85.7	238.3	34	330.5	60.1	7/7	16.5	15.3
XT5	LTC	4.4	82.2	217	29	318.9	56.2	8/8	11.1	17.4
XT4	LTC	337.6	63.6	217	29	323.4	36.7	7/7	11.9	18.3
XT2	LTC	3.4	67.9	217.3	29.7	333.3	44.5	7/7	12.7	17.6
XTC	LTC	278.1	83.0	228.6	26.5	310.0	57.9	5/6	7.1	30.8
XTB	LTC	303.4	72.7	228.6	26.5	312.1	46.6	6/6	19.2	15.7
XTA	LTC	258.3	86.3	228.6	26.5	311.9	61.5	5/6	18.7	18.2
XT6	HTC	265.8	−6.0	238.3	34	258.4	−20.1	7/7	268.4	3.7
XT5	HTC	266.7	15.1	217	29	268.0	−7.4	8/8	50.3	7.9
XT4	HTC	258.0	1.5	217	29	254.9	−17.2	7/7	92.5	6.3
XT2	HTC	265.1	−11.4	217.3	29.7	256.3	−32.1	7/7	60	7.9
XTC	HTC	253.5	−12.6	228.6	26.5	245.6	−22.2	6/6	36.2	11.3
XTB	HTC	259.9	−16.6	228.6	26.5	249.8	−28.5	6/6	106.6	6.5
XTA	HTC	264.6	−24.2	228.6	26.5	250.5	−37.3	6/6	77.7	7.6
Mean	HTC	261.9	−7.8					7/7	34.9	10.4
						255.0	−23.7	7/7	44.1	9.1

Comp, components isolated by principal component analysis (Kirschvink 1980); Dg, Ig and Ds, Is, declination and inclination in geographic and stratigraphic coordinates, respectively; n/N, number of samples (sites) used to calculate the mean direction versus number of samples (sites) measured; κ & α_{95}, Fisher (1953) precision parameter and the half angle of the 95 per cent confidence cone around the mean direction.

directions of Dec = 80.3°, Inc = 26.3°, k= 9.5 and α_{95} = 10.4° in geographic coordinates, and Dec = 77.0°, Inc = 23.3°, k = 34.6 and α_{95} = 5.2° in stratigraphic coordinates. These directions pass McElhinny (1964) fold test at 99 per cent confidence level. In addition, we applied reversal tests (McFadden & McElhinny 1990) for the combined data. The *in situ* normal mean direction and reversed mean direction are Dec = 76.7°, Inc = 38.0°, n = 13, k = 10.0 and Dec = 263.9°, Inc = −11.6°, n = 10, k = 17.2, respectively. The reversal test for the *in situ* mean directions is negative. In stratigraphic coordinates, the normal and reversed mean directions, Dec= 74.9°, Inc = 23.1°, k = 37.8 and Dec = 259.6°, Inc = −23.5°, k = 29.7, pass the reversal test at 95 per cent confidence level. Therefore, both fold test and reversal test suggest that our Early Triassic HTC component is most probably primary.

ROCK MAGNETISM

We performed rock magnetic experiments to provide further constraints on the origin of the ChRM because statistically, any fold test cannot rule out the possibility of a syntectonic remagnetization.

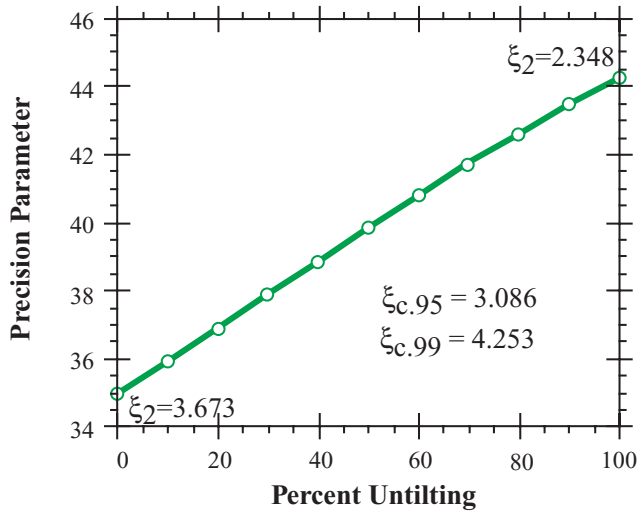

Figure 5. Fold test showing the precision parameter of mean ChRM direction versus percent tilt correction and the statistic parameter ξ_2 of McFadden (1990) fold test. $\xi_{c.95}$ is the critical value at the 95 per cent confidence level. $\xi_2 < \xi_{c.95}$ indicates that the mean direction corresponds to its proper tectonic correction.

Isothermal remanent magnetization (IRM) acquisition experiments show a rapid increase in magnetic moment at low fields (<200 mT), but samples were not completely saturated at the highest applied field (1.2 Tesla), indicating the presence of both low and high coercivity magnetic minerals (Fig. 6a). Thermal demagnetization of two axis orthogonal IRMs (similar to the Lowrie 1990, approach) acquired in 1.2 T and 0.1 T fields shows a steep drop off in the remanence for the low coercivity IRM between 500 and 580 °C (Fig. 6b), suggesting that the low coercivity mineral is dominated by magnetite. The high coercivity IRM component has a more distributed unblocking temperature spectrum, gradually unblocking from 100 to 580 °C; the highest unblocking temperatures is less than 580 °C, also indicative of magnetite. Unblocking of the high coercivity IRM component shows a significant drop-off between 300 and 400 °C, which could indicate the presence of pyrrhotite.

Liquid nitrogen, low temperature (−196 °C) demagnetization of one sample from each site removed 0–5 per cent of the NRM intensity, indicating that single domain (SD) and/or pseudo-single domain (PSD) magnetite is the dominant carrier of the magnetic remanence (e.g. Levi & Merrill 1978; Dunlop & Argyle 1991; Hodych *et al.* 1998). The spectra of partial anhysteretic remanent magnetization (pARM) (Fig. 7) show more or less symmetrical curves with peaks at ∼35 mT, suggesting a single group of magnetite grains in SD or PSD sizes (Jackson *et al.* 1988). The anisotropy of ARM (AARM) measured in the 20–60 mT coercivity window, following McCabe *et al.* (1985) approach, shows no clear relationship with measured structural parameters such as bedding attitudes, stylolites or calcite veins (Fig. 8a). Although replicate AARM tensor measurements were not made, the measurement of AARM tensors for each sample should be accurate because the root mean square error is often less than 0.5 per cent. In addition, the AARM data show low anisotropy (<6 per cent) without clearly defined fabric features; both lineation and foliation values do not exceed 1.06 (Fig. 8b). For SD and PSD magnetite, the AARM data suggest that the effect of tectonic deformation and/or compaction strain on the ChRM direction is negligible.

SEM observation of magnetic extracts from the limestone samples dissolved in sodium acetate buffered, 2M acetic acid reveals

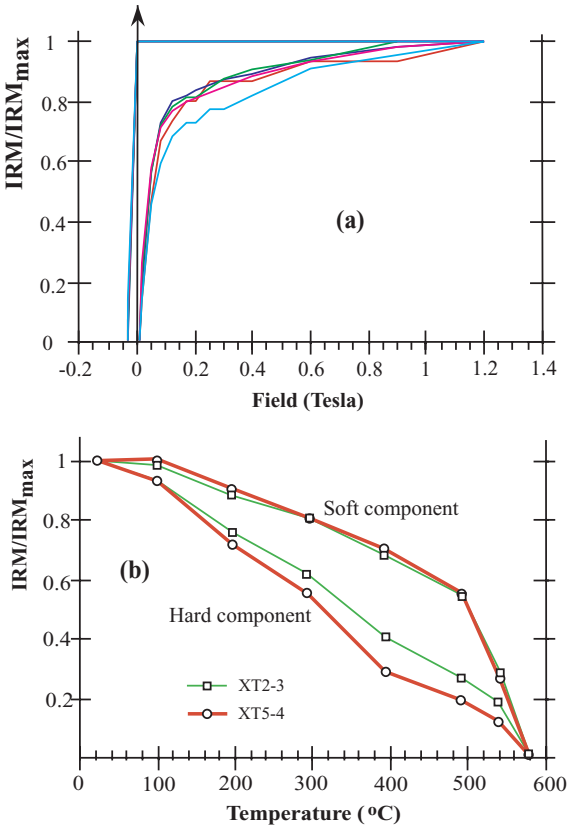

Figure 6. (a) Normalized IRM acquisition and backfield demagnetization curves indicate the presence of both low and high coercivity magnetic minerals. (b) Normalized thermal demagnetization of orthogonal IRM and ARM components suggests that the low coercivity mineral is magnetite, and the high coercivity IRM is carried by magnetite and some minor amount of pyrrhotite.

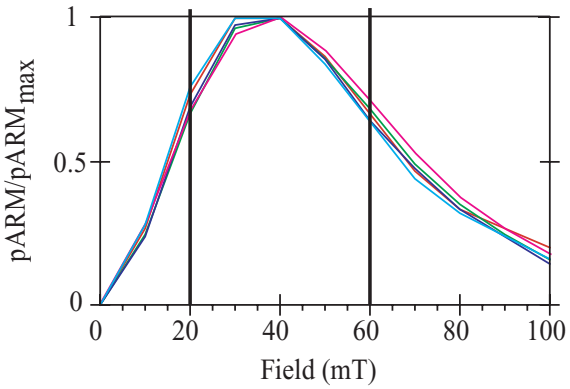

Figure 7. Normalized partial ARM spectra acquired in 10 mT coercivity windows indicate a symmetrical distribution of coercivity spectra, peaking at coercivity of 35 mT.

morphologies similar to magnetite particles formed during Early diagenesis (Fig. 9) (e.g. Hart & Fuller 1988; Schwartz *et al.* 1997) and to those formed through bacteria mediation (Konhauser 1998). Energy dispersion spectrum (EDS) shows little or no titanium content in the magnetic extracts (Fig. 9b), corroborating the diagenetic origin of the magnetic minerals. EDS shows the presence of sulphide minerals, probably pyrrhotite.

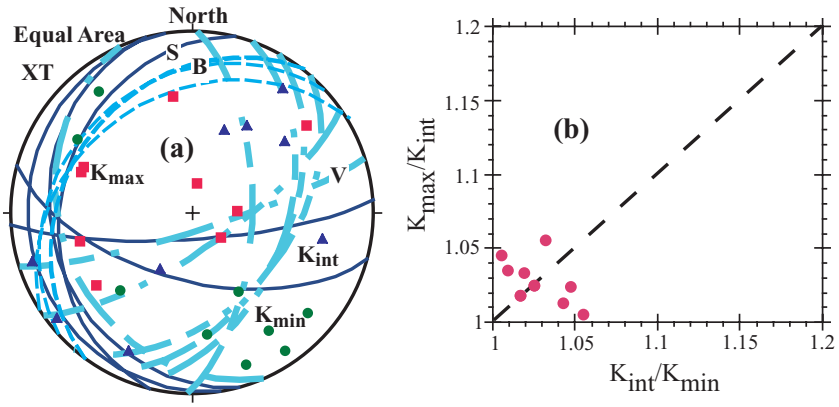

Figure 8. Rock and magnetic fabric results showing (a) equal area projections of bedding planes (B), stylolite planes (S), calcite vein planes (V), and the directions of maximum (square), intermediate (triangle) and minimum axes (circle) of AAR ellipsoids and (b) the shape of AAR ellipsoids (Flinn diagrams).

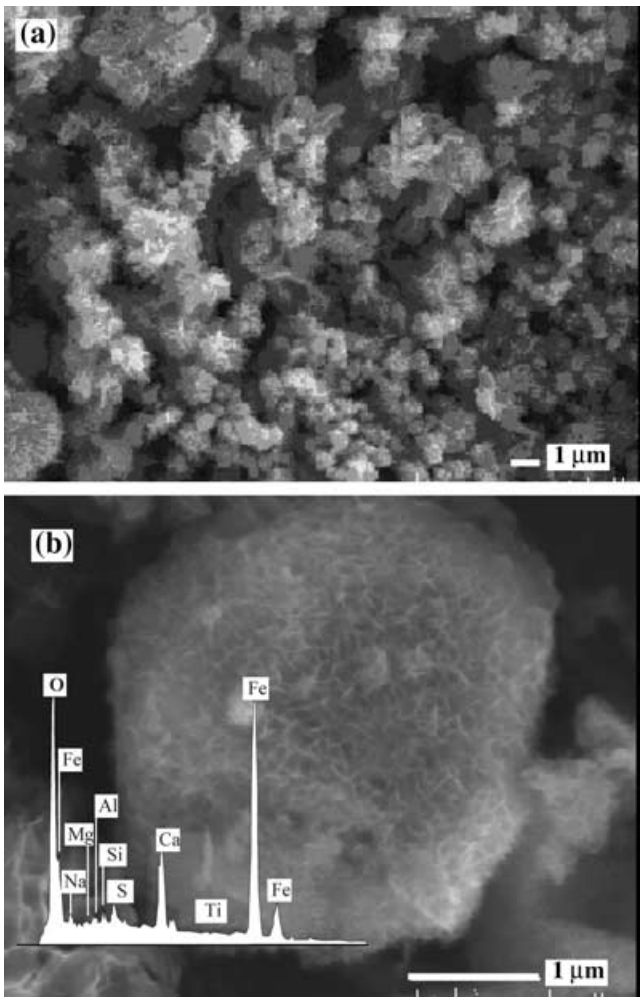

Figure 9. SEM and EDS analyses of magnetic extracts from the limestone samples.

Previous rock magnetic and petrographic studies of remagnetized carbonate rocks suggested that the pARM spectra are biased towards low coercivities (large grain size) and that the magnetite particles are spherical (e.g. McCabe *et al.* 1983, 1989; Lu *et al.* 1990; Tan *et al.* 2000). Our rock magnetic and magnetic fabric data and SEM observations are quite different from those remagnetized examples, and together with the positive fold test, suggest that the age of the ChRM is very close to the age of diagenesis. Moreover, the lack of significant magnetic anisotropy suggests that the ChRM directions have not been affected by compaction or tectonic strain.

DISCUSSION

A clockwise rotation pattern in the Middle Yangtze fold belt

Fold and thrust belts are often curved in map view. Based on the presence or absence of relative rotation that is coherent with the curved pattern within the fold belt, the curvature can be divided into rotational or non-rotational parts (e.g. Marshak 1988). The rotated part of the curved fold belt is defined as an orocline, and the process leading to the rotation is called oroclinal bending (Carey 1955). Identifying the relative rotation pattern in time and space can then better elucidate the various scales of deformation processes of the fold belt. A commonly used way to study their formation is to compare palaeomagnetic declinations with fold axis trends at several places along the curvature of the fold belt (e.g. Schwartz & Van der Voo 1983; Butler *et al.* 1995). In the correlation analysis of declinations and fold axis strikes, it is assumed that the fold axes were initially more or less consistent throughout the fold belt. Because the correlation analysis can be flawed by initial changes in fold axis trends, initial variations of fold axis strikes should be taken into account wherever possible. In addition, small rotations can be overwhelmed by large declination values, leading to less significant tests. Therefore, relative rotations with respect to the expected declinations instead of measured palaeomagnetic declinations at various localities should be used in a more accurate analysis of the relationship between palaeomagnetic rotations and fold axis strikes.

Our Early Triassic palaeomagnetic declination is consistent at the 95 per cent confidence interval with the Middle Triassic declination of Huang & Opdyke (1996) from the Badong section; these two sections (Badong and Xiangxi) have rotated clockwise by $29^\circ \pm 8^\circ$ and $31^\circ \pm 8^\circ$ with respect to the reference palaeomagnetic declinations, respectively. This coherent rotation may exclude the possibility of a local scale, vertical axis rotation for any one of the sections and suggests that the 100 km long, E–W trending Badong–Xiangxi segment of fold belt has probably rotated in the same manner as a single unit (Fig. 1b). There is a 45° difference in fold axis trend between the Badong–Xiangxi segment of the fold belt and the NE–SW trending

fold belt, whereas the rotation could only account for two thirds of the difference. Therefore, the fold axis trends might initially have a 15° offset with the Badong–Xiangxi segment trending more easterly.

To further analyse the rotation pattern in the Yangtze fold belt, we plotted the relative rotation amount (Rt) against the fold axis trend (Fig. 10, Table 2). There is no relationship between these two

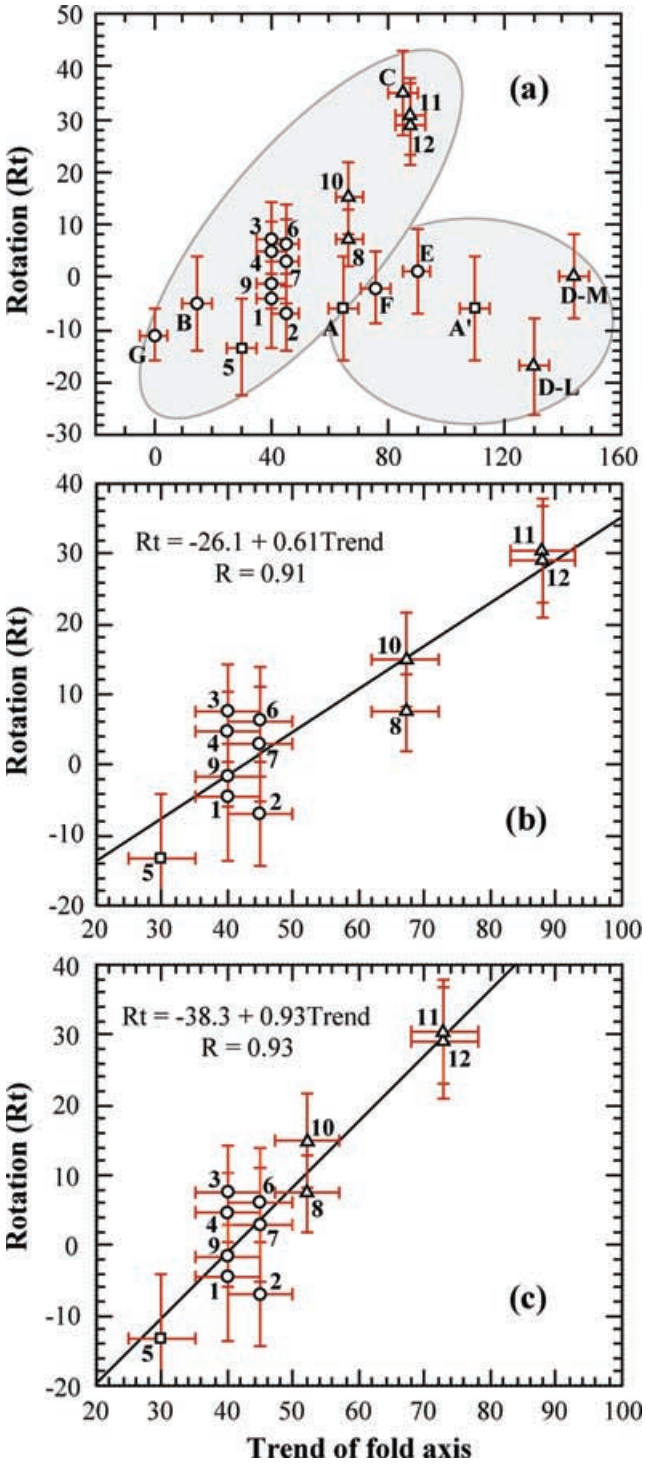

Figure 10. Plots showing the correlation between palaeomagnetic rotation and the trend of fold axis. (a) All data from the Yangtze fold belt; (b) analysis of one group of data in (a) and (c) analysis of the same data as (b) but with adjustment of the trends of fold axes for the two mid-Yangtze localities (Nos. 8, 10–12 in Table 2 and region III in Fig. 1b).

parameters for the whole data set (Fig. 10a). However, it appears that there are two groups of data. In one group, Rt is significantly correlated with the fold axis strikes ($R = 0.9$) (Fig. 10b). However, since the slope is not equal to one there are other factors contributing to the variation of the data. Considering the fact that the most significantly rotated data are from the mid-Yangtze fold belt, they might also have had initially more easterly orientations of the fold axis, as in the Badong–Xiangxi segment. When a 15° is subtracted from the fold axis trends for data in the mid-Yangtze region, the relationship between Rt and fold axis trend is linear with a factor of one. This group of data thus apparently supports a general clockwise rotation pattern in the Middle Yangtze fold belt.

The other group of data that essentially show no significant rotation are from the Lower Yangtze and the northwestern corner of the fold belt. The data from the Middle Yangtze that show no significant rotation came from the Jinmeng–Dangyang basin and from Puqi located at the far eastern part of the E–W trending folds in the Middle Yangtze. However, there is no straightforward interpretation for these data. Huang & Opdyke (1997) interpreted the bedding from Puqi as overturned. However, when we applied an incremental fold test to the data assuming overturned beds, the precision parameter maximized at 35 per cent unfolding with a corresponding direction at Dec = 99°, Inc = 32° ($\alpha_{95} = 6°$, $N = 7$). The test is significant at the 95 per cent confidence level (McFadden 1990). The geometry at 35 per cent untilting coincides with that assuming normal, not overturned beds. Therefore, either the strata are overturned and the palaeomagnetic direction is a synfolding remagnetization, or the strata are not overturned and the ChRM is pre-folding. In either case, the remanent magnetization shows a significant clockwise rotation.

The data (D, Table 2) from the Jingmen–Dangyang basin, Hubei were collected from two sections in a complex geological structure (Huang & Opdyke 1997). The basin is bounded by a group of NNW-SSE trending thrust faults to the east, a normal fault to the west, and one EW trending thrust fault to the north (Fig. 1c). The strata from the Maoping (M on Fig. 1c) section dip gently and their strikes are parallel to the trends of nearby normal faults. It appears that tilting of Maoping strata was related to normal faulting in the region, a later and different tectonic episode from the NS directed convergence that could have possibly caused significant clockwise rotation in mid-Yangtze region. The Liujiatai (L on Fig. 1c) section is situated at the south limb of a NW–SE trending fold and is bounded by a dextral strike-slip fault to the SE. Since the strikes of Liujiatai beds are oblique to the fold axis, the section might have been rotated during strike-slip faulting, and the palaeomagnetic declination of the Maoping section might not be representative of the fold. In addition, the structure in the basin appears to be a second-order feature, not coherent with the general EW trending folds in the mid-Yangtze.

Causes for the clockwise rotation in the mid-Yangtze fold belt

Steiner *et al.* (1989) interpreted a minor clockwise rotation observed in their Permo-Triassic rocks from the Upper Yangtze fold belt as due to oroclinal bending of the fold belt. Huang & Opdyke (1996) observed more clockwise rotations from the Middle Yangtze fold belt, and attributed them to a broader orocline. In a strict sense, rotation should occur after folding in an orocline. Although the correlation between palaeomagnetic rotation and fold axis trend is significant (Figs 10b and c), suggesting that an oroclinal bending of the fold belt is possible, at this point, there is little evidence

Table 2. Late Permian and Triassic palaeomagnetic directions from the South China Block.

No.	Locality	Coordinates (°N/°E)	Mean direction Dec/Inc(α_{95})(°)	Strike (N°E)	Age	Dr(°)	Rt(°)	Reference
1	Tongzi, Guizhou	28.6/106.9	40/13(11)	40	T_E	44 ± 4	-4 ± 9	a
A	Nanjin, Jiangsu	32.0/119.0	45/24(9)	65/110	T_M	51 ± 6	-6 ± 10	a
2	Guangyuan, Sichuan	32.4/106.4	36/12(4)	45	$P_L - T_E$	43 ± 8	-7 ± 9	b
3	Hechuan, Sichuan	29.9/106.3	50/17(3)	40	$P_L - T_E$	43 ± 8	7 ± 8	b
4	Hechuan, Sichuan	29.9/106.3	49/15(6)	40	T_E	44 ± 4	5 ± 6	b
B	Liangfengya, Sichuan	29.6/105.6	37/6(5)	15	$P_L - T_E$	42 ± 8	-5 ± 9	b
5	Changxing, Zhejiang	31.0/119.8	36/23(11)	30	T_E	49 ± 4	-13 ± 10	c
6	Changshou, Sichuan	29.9/107.0	49/17(5)	45	$P_L - T_E$	43 ± 8	6 ± 9	d
7	Nanxi, Sichuan	28.9/104.9	45/17(6)	45	$P_L - T_E$	42 ± 8	3 ± 9	d
8	Sangzhi, Hunan	29.4/110.2	53/29(6)	67	T_{E-M}	46 ± 4	7 ± 6	e
9	Shuijiang, Sichuan	29.3/107.3	43/15(4)	40	T_E	45 ± 4	-2 ± 5	f
10	Sangzhi, Hunan	29.4/110.2	62/27(6)	67	T_M	47 ± 6	15 ± 8	g
11	Badong, Hubei	31/110.4	78/23(7)	88	T_M	47 ± 6	31 ± 8	g
C	Puqi, Hubei	29.7/113.9	99/32(6)	85	?	≤ 50	≥ 35	g
D-L	JingDang, Hubei	31.4/111.7	31/27(9)	130	T_M	48 ± 6	-17 ± 9	h
D-M	JingDang, Hubei	31.4/111.7	48/24(6)	144	T_M	48 ± 6	0 ± 8	h
E	Wangcang, Sichuan	32.1/106.2	45/18(9)	90(?)	T_E	44 ± 4	1 ± 8	i
12	Xiangxi, Hubei	31/110.8	75/24(9)	88	T_E	46 ± 4	29 ± 8	This study
F	Xuyong, Sichuan	28/105.5	42/10(7)	76(?)	T_E	44 ± 4	-2 ± 7	j
G	Panxi, Yunnan	28.2/103	32/26(5)	0	T_E	43 ± 4	-11 ± 5	k
H	Yufeng, Guangxi	23.6/107.2	56/7(10)	133	T_M	45 ± 6	11 ± 10	l
I	Emei, Sichuan	29.6/103.4	37/14(3)	?	T_E	43 ± 4	-6 ± 4	m
J	Yueshan, Anhui	30.64/116.93	12/34(4)	?	T_M	50 ± 6	-38 ± 7	n
		30.64/116.83	281/35(6)	?	T_M	50 ± 6	231 ± 8	n
		30.24/116.5	285/38(18)	?	T_M	50 ± 6	236 ± 16	n
K	Lianxian, Guangdong	24.2/117.9	18/20(9)	?	T_E	47 ± 4	-29 ± 8	o
		24.2/118.2	114/12(12)	?	?			o

Results listed in Arabic numbers are shown in Fig. 1(b). The correlation between relative palaeomagnetic rotation and the fold axis trend are analysed in Figs 10(b) and (c). Results listed in letters are not used for the correlation analysis (see discussion in text). Strike, is the strike of fold axes; Dr, the reference declinations with 95 per cent confidence limits calculated for various localities from reference poles; Rt, degree of rotation with respect to the expected declination. The reference poles are 42.7°N, 212.6°E ($A_{95} = 6°$), 43.8°N, 213.8°E ($A_{95} = 3.5°$) and 43.4°N, 218.4°E ($A_{95} = 8.1°$) for T_M, T_E (Yang & Besse 2001) and $P_L - T_E$ (Gilder & Courtillot 1997), respectively. T_M, Middle Triassic; T_E, Early Triassic; $P_L - T_E$, Latest Permian and Earliest Triassic. Reference: (a) Opdyke *et al.* (1986); (b) Steiner *et al.* (1989); (c) Dobson *et al.* (1993); (d) Enkin *et al.* (1992); (e) Dobson & Heller (1993); (f) Heller *et al.* (1995); (g and h) Huang & Opdyke (1996, 1997); (i) Bai *et al.* (1997); (j) Yang & Besse (2001); (k) Zhu *et al.* (1988); (l) Gilder *et al.* (1995); (m) Ma & Zhang (1989); (n) Gilder *et al.* (1999) and (o) Tan *et al.* (2000).

to prove or disapprove an orocline hypothesis because we do not know the timing of the clockwise rotation, whether it happened before, during or after folding. In either case, a wholesale rotation would not change the distribution and cluster pattern of the palaeomagnetic data. Although passing fold tests, the palaeomagnetic results do not necessarily indicate rotations happened before folding. Therefore, the more detailed deformation processes have yet to be unveiled.

Our understanding of the concept of orocline is that a part of fold belt that may be initially more or less linear was subjected to relative rotation into its present orientation. Orocline implies a specific deformation process involving folding and subsequent rotation, a view shared by Stamatakos & Hirt (1994). In a study of the origin of the Pennsylvania salient in the central Appalachians, Stamatakos & Hirt (1994) found that the Permian synfolding remagnetization directions are consistent throughout the salient. Although the Silurian, Devonian and Carboniferous palaeomagnetic declinations from the northeastern and southwestern limbs of the salient are consistent with an orocline model for the formation of the Pennsylvania salient (e.g. Kent 1988; Stamatakos & Hirt 1994), Stamatakos & Hirt (1994) concluded that the curvature in the salient is not caused by oroclinal bending and the observed rotation happened before folding of the central Appalachians. The Yangtze fold belt might have a long-lasted, complex deformation history because NCB–SCB collision started in Late Permian and lasted till Middle/Late Jurassic (e.g. Zhao & Coe 1987; Gilder & Courtillot 1997). So far, the rotated palaeomagnetic data are from the Early and Middle Triassic rocks, providing a post-Middle Triassic age for the rotation event. Because the folding occurred during the Middle and Late Jurassic (BGMRHP 1990), the observed rotation could have happened before folding. Therefore, a firm conclusion for oroclinal bending in the Middle Yangtze fold belt cannot be drawn from the observed clockwise rotation until more data, especially synfolding magnetization components are available.

The deformation, particularly the clockwise rotation in the Middle Yangtze fold belt can be readily explained by the indentation of the NCB into the SCB (Okay *et al.* 1993; Gilder *et al.* 1999). However, palaeomagnetic data from Puqi and the Jingmen–Dangyang basin led Huang & Opdyke (1997) to seek another cause for the observed clockwise rotation in the Middle Yangtze fold belt. Their rationale is that, if the observed palaeomagnetic rotations were caused by the NCB–SCB collision, the Jingmen–Dangyang basin, which is close to the collision boundary, should also have experienced significant rotations. Otherwise, the observed block rotations should not be related to the collision. Because their data from the Puqi section and the Jingmen-Dangyang basin showed no significant rotation, they concluded that the clockwise rotation pattern in the Middle Yangtze region was not caused by the NCB–SCB collision. Instead, they attributed the clockwise rotation to the collision between Yangtze and Huanan blocks (e.g. Hsu *et al.* 1988), compres-

sion related to the subduction of the Pacific Plate, and/or accretion of minor suspect terranes.

We propose two alternative interpretations for the palaeomagnetic data from the Jingmen–Dangyang basin (Huang & Opdyke 1997), which could be consistent with NCB–SCB collision. The first may be described by back rotation of the sampled section. The fold axis direction has a 130° azimuth, but the bedding strikes, ranging from 55° to 88°, averaging at 72°, are oblique to the fold axis. The palaeomagnetic declination of the Liujiatai section is 31°. If the Liujiatai section was rotated 58° counter-clockwise during dextral strike-slip faulting following folding, recovery of this back rotation will bring bedding strikes consistent with the fold axis, and the restored palaeomagnetic declination will be 89°. This would suggest a 41° clockwise rotation and 41° initial orientation of the fold axis. Second, the discrepancy might be attributed to the way in which deformation was partitioned. The Jingmen–Dangyang part of the fold belt is bounded on all sides by faults (Fig. 1c) and only Triassic strata were involved in deformation, probably suggesting that this thin-skinned sheet was first detached and overthrusted, with folding occurring at the latest stage of the NCB–SCB convergence so that these folds avoided significant rotation. Further work in this area can test these two possibilities.

The convergence direction among various blocks might be indicative of the causes for the deformation in the Middle Yangtze fold belt. The convergence between NCB and SCB was generally N–S directed, whereas the postulated convergence between Yangtze and Huanan Blocks and the subduction of the Pacific Plate into South China are northwest directed. The latter should yield NE–SW trending tectonic trajectories, like the intrusive and extrusive volcanic chains observed in South China. The Middle Yangtze fold belt is dominated by an E–W trending trajectory, apparently linking to the N–S directed convergence between NCB and SCB.

CONCLUSION

A palaeomagnetic study of the Early Triassic Daye Formation limestones yielded a stable HTC direction, which passes fold test and consistency test. Rock magnetic data suggest that acquisition of the HTC is very close to the age of sedimentation and show that the effect of strain on the HTC direction is negligible. Our new direction is consistent with previously reported easterly Middle Triassic directions from the Middle Yangtze region. To a larger extent, there is a general clockwise rotation pattern in the Middle Yangtze fold belt, which was probably caused by the NCB–SCB collision. Further studies are needed to reveal the detailed deformation processes leading to the clockwise rotation in the region.

ACKNOWLEDGMENTS

We are grateful to Prof Meng Fanseng, at Yichang Institute of Geology and Mineral Resources, Chinese Academy of Geological Sciences, for his guidance to the outcrops. Comments from Rob Van der Voo and an anonymous reviewer, and suggestions from the journal editor Erwin Appel have improved the manuscript. This study was supported by the National Natural Science Foundation of China (40374023), and the US NSF (EAR-9315778). This is IPGP contribution no. 2158.

REFERENCES

Academia Sinica, 1976. *Geological Map of China, scale 1:4,000,000*, Geol. Publ. House, Beijing.

Bai, L., Wu, H. & Zhu, R., 1997. Palaeomagnetic result of the Early Triassic from the Wangcang area in north Sichuan, *Sci. China Ser. D,* **27,** 514–520.

Bureau of Geology and Mineral Resources of Hubei Province (BGMRHP), 1990. *Regional Geology of Hubei Province* (in Chinese), Geological Memoirs Series 1, No. 20, Geol. Publ. House, Beijing, p. 705.

Bureau of Geology and Mineral Resources of Sichuan Province (BGMRSP), 1991. *Regional Geology of Sichuan Province* (in Chinese), Geological Memoirs Series 1, No. 23, Geol. Publ. House, Beijing, p. 730.

Butler, R.F., Richards, D.R., Sempere, T. & Marshall, L.G., 1995. Palaeomagnetic determinations of vertical-axis tectonic rotations from Late Cretaceous and Palaeocene strata of Bolivia, *Geology,* **23,** 799–802.

Carey, S.W., 1955. The orocline concept in geotectonics, *Pap. Proc. R. Soc. Tasmania,* **89,** 255–289.

Dobson, J.P. & Heller, F., 1993. Triassic palaeomagnetic results from the Yangtze Block, S.E. China, *Geophys. Res. Lett.,* **20,** 1391–1394.

Dobson, J.P., Heller, F., Li, Z. & Mauritsch, H., 1993. Palaeomagnetic and rock magnetic investigations of the Changxing Permian-Triassic section, Zhejiang province, China, *Geophys. Res. Lett.,* **20,** 1667–1670.

Dunlop, D.J. & Argyle, K.S., 1991. Separating multidomain and single-domain-like remanence in pseudo-single-domain magnetites (215–540 nm) by low temperature demagnetization, *J. geophys. Res.,* **96,** 2007–2017.

Enkin, R.J., 1990. *Formation et deformation de l'Asie depuis la fin de l'ere primaire, les apports de l'étude paléomagnétique des formations secondaires de Chine du Sud*, These de Doctorat de l'Universite Paris 7, p. 333.

Enkin, R.J., 2003. The direction-correction tilt test: an all-purpose tilt/fold test for palaeomagnetic studies, *Earth planet. Sci. Lett.,* **212,** 151–166.

Enkin, R.J., Yang, Z., Chen, Y. & Courtillot, V., 1992. Palaeomagnetic constraints on the geodynamic history of the major blocks of China from the Permian to present, *J. geophys. Res.,* **97,** 13 953–13 989.

Fang, D., Tan, X., Guo, Y. & Yu, G., 1990. Palaeomagnetism and tectonic evolution in Mesozoic for North China Plate, in *Terrane Analysis of China and the Pacific Rim*, pp. 359–363, eds Wiley, T.J., Howell, D.G. & Wong, F.L., Circum-Pacific Council for Energy and Mineral Resources, Earth Science Series 13.

Fisher, R.A., 1953. Dispersion on a sphere, *Proc. R. Soc. London* A, **217,** 295–305.

Gilder, S. & Courtillot, V., 1997. Timing of the North-South China collision from new Middle to Late Mesozoic palaeomagnetic data from the North China Block, *J. geophys. Res.,* **102,** 17 713–17 727.

Gilder, S., Coe, R., Wu, H., Kuang, G., Zhao, X. & Wu, Q., 1995. Triassic palaeomagnetic data from south China and their bearing on the tectonic evolution of the western circum-Pacific region, *Earth planet. Sci. Lett.,* **131,** 269–287.

Gilder, S. *et al.*, 1999. Tectonic evolution of the Tancheng-Lujiang (Tan-Lu) fault via Middle Triassic to Early Cenozoic palaeomagnetic data, *J. geophys. Res.,* **104,** 15 365–15 390.

Hart, M. & Fuller, M., 1988. Magnetization of a dolomite bed in the Monterey Formation; implications for diagenesis, *Geophys. Res. Lett.,* **15,** 491–494.

Heller, F., Chen, H., Dobson, J. & Haag, M., 1995. Permian-Triassic magnetostratigraphy: new results from south China, *Phys. Earth planet. Inter.,* **89,** 281–295.

Hodych, J.P., Mackay, R.I. & English, G.M., 1998. Low-temperature demagnetization of saturation remanence in magnetite-bearing dolerites of high coercivity, *Geophys. J. Int.,* **132,** 401–411.

Hsu, K.J., Sun, S., Li, J.L., Chen, H.H., Pen, H.R. & Sengör, A.M.C., 1988. Mesozoic thrust tectonics in south China, *Geology,* **16,** 418–421.

Huang, K. & Opdyke, N.D., 1996. Palaeomagnetism of Middle Triassic redbeds from Hubei and northwestern Hunan provinces, South China, *Earth planet. Sci. Lett.,* **143,** 63–79.

Huang, K. & Opdyke, N.D., 1997. Middle Triassic palaeomagnetic results from central Hubei province, China and their tectonic implications, *Geophys. Res. Lett.,* **24,** 1571–1574.

Jackson, M., Gruber, W., Marvin, J. & Banerjee, S.K., 1988. Partial anhysteretic remanence and its anisotropy: applications and grain size-dependence, *Geophys. Res. Lett.,* **15,** 440–443.

Kent, D.V., 1988. Further palaeomagnetic evidence for oroclinal rotation in the central folded Appalachians from the Bloomsburg and the Mauch Chunk Formations, *Tectonics,* **7,** 749–759.

Kirschvink, J.L., 1980. The least-square line and plane and the analysis of palaeomagnetic data, *Geophys. J. R. astr. Soc.,* **62,** 699–712.

Konhauser, K.O., 1998. Diversity of bacterial iron mineralization, *Earth-Sci. Rev.,* **43,** 91–121.

Levi, S. & Merrill, R.T., 1978. Properties of single-domain, pseudo-single-domain and multidomain magnetite, *J. geophys. Res.,* **83,** 309–323.

Lin, J.-L., Fuller, M. & Zhang, W.-Y., 1985. Preliminary Phanerozoic polar wander paths for the North and South China blocks, *Nature,* **313,** 444–449.

Lowrie, W., 1990. Identification of ferromagnetic minerals in a rock by coercivity and unblocking temperature properties, *Geophys. Res. Lett.,* **17,** 159–162.

Lu, G., Marshak, S. & Kent, D.V., 1990. Characteristics of magnetic carriers responsible for Late Palaeozoic remagnetization in carbonate strata of the mid-continent, USA, *Earth planet. Sci. Lett.,* **99,** 351–361.

Ma, X. & Zhang, Z., 1989. Palaeomagnetic study of Permian rocks from Sichuan Emei region and Shanxi Taiyuan region, *Acta Geophys. Sin.,* **32,** 451–465.

Marshak, S., 1988. Kinematics of orocline and arc formation in thin-skinned orogens, *Tectonics,* **7,** 73–86.

McCabe, C., Van der Voo, R., Peacor, D.R., Scotese, C.R. & Freeman, R., 1983. Diagenetic magnetite carries ancient yet secondary remanence in some Palaeozoic sedimentary carbonates, *Geology,* **11,** 221–224.

McCabe, C., Jackson, M. & Ellwood, B.B., 1985. Magnetic anisotropy in the Trenton limestone: results of a new technique, anisotropy of anhysteretic susceptibility, *Geophys. Res. Lett.,* **12,** 333–336.

McCabe, C., Jackson, M. & Saffer, B., 1989. Regional patterns of magnetite authigenesis in the Appalachian basin: implications for the mechanism of Late Palaeozoic remagnetization, *J. geophys. Res.,* **94,** 10 429–10 443.

McElhinny, M.W., 1964. Statistical significance of the fold test in palaeomagnetism, *Geophys. J. R. astr. Soc.,* **8,** 338–340.

McElhinny, M.W., Embleton, B.J.J., Ma, X. & Zhang, Z., 1981. Fragmentation of Asia in the Permian, *Nature,* **293,** 212–216.

McFadden, P.L., 1990. A new fold test for palaeomagnetic studies, *Geophys. J. Int.,* **103,** 163–169.

McFadden, P.L. & McElhinny, M.W., 1990. Classification of the reversal test in palaeomagnetism, *Geophys. J. Int.,* **103,** 725–729.

Okay, A.I., Sengör, A.M.C. & Satir, M., 1993. Tectonics of an ultrahigh-pressure metamorphic terrane: the Dabie Shan/Tongbai Shan orogen, China, *Tectonics,* **12,** 1320–1334.

Opdyke, N.D., Huang, K., Xu., G., Zhang, W. & Kent, D.V., 1986. Palaeomagnetic results from the Triassic of the Yangtze platform, *J. geophys. Res.,* **91,** 9553–9568.

Schwartz, M., Lund, S.P., Hammond, D.E., Schwartz, R. & Wong, K., 1997. Early sediment diagenesis on the Blake/Bahama outer ridge, North Atlantic Ocean, and its effects on sediment magnetism, *J. geophys. Res.,* **102,** 7903–7914.

Schwartz, S.Y. & Van der Voo, R., 1983. Palaeomagnetic evaluation of the orocline hypothesis in the central and southern Appalachians, *Geophys. Res. Lett.,* **10,** 505–508.

Stamatakos, J. & Hirt, A.M., 1994. Palaeomagnetic considerations of the development of the Pennsylvania salient in the central Appalachians, *Tectonophysics,* **231,** 237–255.

Steiner, M., Ogg, J., Zhang, Z. & Sun, S., 1989. The Late Permian/Early Triassic magnetic polarity time scale and plate motions of China, *J. geophys. Res.,* **94,** 7343–7363.

Tan, X., Kodama, K.P., Wang, P. & Fang, D., 2000. Palaeomagnetism of Early Triassic limestones from the Huanan Block, South China: no evidence for separation between the Huanan and Yangtze blocks during the Early Mesozoic, *Geophys. J. Int.,* **142,** 241–256.

Watson, G.S. & Enkin, R.J., 1993. The fold test in palaeomagnetism as a parameter estimation problem, *Geophys. Res. Lett.,* **20,** 2135–2137.

Xu, J., 1993. Basic characteristics and tectonic evolution of the Tancheng-Lujiang Fault zone, in *The Tancheng-Lujiang Wrench Fault System*, pp. 17–50, ed Xu, J., John Wiley & Sons, New York.

Yang, Z. & Besse, J., 2001. New Mesozoic apparent polar wander path for south China: Tectonic consequences, *J. geophys. Res.,* **106,** 8493–8520.

Yang, Z.Y., Chen, Y.Q. & Wang, H.Z., 1986. *The Geology of China*, Clarendon Press, Oxford, 303 pp.

Yang, Z., Ma, X.H., Besse, J., Courtillot, V., Xing, L., Xu, S. & Zhang, J., 1991. Palaeomagnetic results from Triassic sections in the Ordos basin, North China, *Earth planet. Sci. Lett.,* **104,** 258–277.

Yang, Z., Courtillot, V., Besse, J., Ma, X., Xing, L., Xu, S. & Zhang, J., 1992. Jurassic palaeomagnetic constrains on the collision of the North and South China blocks, *Geophys. Res. Lett.,* **19,** 577–580.

Zhao, X.X. & Coe, R.S., 1987. Palaeomagnetic constrains on the collision and rotation of north and south China, *Nature,* **327,** 141–144.

Zhu, Z.W., Hao, T. & Zhao, H., 1988. Palaeomagnetic study on the tectonic motion of Pan-Xi block and adjacent area during Yin Zhi-Yanshan period, *Acta Geophys. Sin.,* **31,** 420–431.

Zijderveld, J.D.A., 1967. A.C. demagnetization of rocks: analysis of results, in *Methods in Palaeomagnetism*, pp. 254–286, eds Collison, D.W., Crèer, K.M. & Runcorn, S.K., Elsevier, New York.